Remote Sensing of Environment 159 (2015) 57–69

Contents lists available at ScienceDirect

Remote Sensing of Environment

journal homepage: www.elsevier.com/locate/rse

Evaluating EO-based canopy water stress from seasonally detrended NDVI and SIWSI with modeled evapotranspiration in the Senegal River Basin

Jørgen L. Olsen [a,*], Simon Stisen [b], Simon R. Proud [a], Rasmus Fensholt [a]

[a] Department Geosciences and Natural Resource Management, University of Copenhagen, Øster Voldgade 10, DK-1350 Copenhagen K, Denmark
[b] Geological Survey of Denmark and Greenland (GEUS), Øster Voldgade 10, DK-1350 Copenhagen K, Denmark

ARTICLE INFO

Article history:
Received 28 March 2014
Received in revised form 20 November 2014
Accepted 25 November 2014
Available online 6 January 2015

Keywords:
Geostationary
MSG
Drought
MIKESHE modeling
Sahel
Drylands

ABSTRACT

Satellite remote sensing of vegetation parameters and stress is a key issue for semi-arid areas such as the Sahel, where vegetation is an important part of the natural resource base. In this study we examine if additional information can be obtained on intra-seasonal short term scale by using the Shortwave Infrared Water Stress Index (SIWSI) as compared to Normalized Difference Vegetation Index (NDVI). We perform a spatio-temporal evaluation of NDVI and SIWSI using geostationary remote sensing imagery from the Spinning Enhanced Visible and Infrared Imager (SEVIRI). The indices and their seasonally detrended anomalies are evaluated using a gridded rainfall product (RFE2) and modeled actual evapotranspiration (ETa) for the Senegal River basin in 2008. Daily NDVI and SIWSI were found spatially highly correlated to ETa with $r = 0.73$ for both indices, showing the importance of the north/south vegetation gradient in the river catchment. The hypothesis that short term evolution of index anomalies are related to canopy water status was tested by comparing 10-day averages of ETa with short term changes in daily NDVI and SIWSI anomalies, and moderate to strong coefficients of determination where found when anomaly variations where aggregated by Land Cover Classes (LCCs) with R^2 values of 0.65 for savanna, 0.60 for grassland, 0.72 for shrubland, and 0.58 for barren or sparsely vegetated areas. This is higher than for the same method applied to NDVI anomalies, with R^2 values of 0.57 for savanna, 0.50 for grassland, 0.32 for shrubland, and 0.57 for barren or sparsely vegetated areas. The approach of detrending NIR/SWIR based indices and spatially aggregating the anomalies do offer improved detection of intra-seasonal stress. However, quite coarse spatial aggregation is found necessary for a significant analysis outcome.

1. Introduction

Satellite remote sensing of terrestrial vegetation and vegetation status provides essential information for natural resource management and drought early warning systems in global dryland areas (Fensholt et al., 2012). The semi-arid Sahel in Sub-Saharan Africa is amongst the world's largest dryland areas, yet characterized by limited availability of conventional meteorological ground observations. This makes Earth observation (EO) based vegetation monitoring particularly useful. In the Sahel, vegetation growth is highly related to rainfall (Nicholson, Davenport, & Malo, 1990), and rainfall variability is a major challenge for the sustainability of local livelihoods (Mertz et al., 2012).

Many indices have been proposed to study and monitor vegetation health and vigor using information from visible (VIS), near infrared (NIR), and shortwave infrared (SWIR) spectral bands. The most widely applied of these indices is the Normalized Difference Vegetation Index (NDVI), which has been found related to several vegetation parameters like photosynthetic activity, fractional vegetation cover, and Net Primary Production (NPP) (Carlson & Ripley, 1997; Prince, 1991a,b; Tucker, 1979). NDVI has been used to assess changes in phenology and long term vegetation trends using datasets such as the Global Inventory Modeling and Mapping Studies (GIMMS) data from the Advanced Very High Resolution Radiometer (AVHRR) (Fensholt, Sandholt, Rasmussen, Stisen, & Diouf, 2006; Fensholt et al., 2012; Heumann, Seaquist, Eklundh, & Jonsson, 2007; Julien & Sobrino, 2009; Sobrino & Julien, 2011), which now spans several decades.

NDVI is also commonly combined with information in the Thermal Infrared (TIR) spectrum for drought monitoring (Carlson & Ripley, 1994; Gillies, Carlson, Cui, Kustas, & Humes, 1997; Sandholt, Rasmussen, & Andersen, 2002). The Vegetation Health Index (VHI) (Kogan, 1995) combines NDVI and the Temperature Condition Index (TCI) from AVHRR reflectances and brightness temperatures. VHI has recently been applied for agricultural drought probability mapping of the African continent (Rojas, Vrieling, & Rembold, 2011), thus avoiding the use of potentially unreliable gridded rainfall datasets. Furthermore, the high dependency and sensitivity of vegetation to rainfall in the Sahel has lead studies to suggest using NDVI as a proxy for rainfall to

* Corresponding author.
E-mail address: jlo@ign.ku.dk (J.L. Olsen).

http://dx.doi.org/10.1016/j.rse.2014.11.029
0034-4257/

compensate for unreliable rainfall data (Anyamba & Tucker, 2005; Proud & Rasmussen, 2010). Although studies of the impact of inter-annual rainfall variability on vegetation indices are most common, NDVI has also been applied in studies on intra-annual timescale of vegetation response to seasonal rainfall patterns e.g. in the Sahel (Proud & Rasmussen, 2010), using data from the Spinning Enhanced Visible and Infrared Imager (SEVIRI) onboard the geostationary Meteosat Second Generation (MSG) platform, and in Kansas (Wang, Rich, & Price, 2003) using AVHRR data.

While NDVI has been found suitable for inter-annual studies on a relatively coarse temporal and spatial resolution in a multitude of studies (Fensholt & Proud, 2012), the red and NIR based NDVI is not necessarily the most useful index for providing information on short term variations in surface water properties, like evapotranspiration, caused by changing water availability and canopy water content. Due to the SWIR spectrum's sensitivity to the amount of liquid water in the canopy (Tucker, 1978; Tucker, 1980), several NIR/SWIR based indices sensitive to canopy water content have been examined for their applicability (Ceccato, Flasse, Tarantola, Jacquemoud, & Gregoire, 2001; Ceccato, Gobron, Flasse, Pinty, & Tarantola, 2002; Ceccato, Flasse & Gregoire, 2002; Fensholt & Sandholt, 2003; Gao, 1996). Amongst these the Shortwave Infrared Water Stress Index (SIWSI) has been studied in a Sahelian context. The evolution of SIWSI over a growing season has been shown to be highly related to the evolution of growing season NDVI, but SIWSI has also proved to be sensitive to short-term changes in canopy water status (i.e. whether the canopy is water stressed or not). This was shown from comparison with observed and modeled soil moisture in northern Senegal, where the SIWSI signal for a herbaceous canopy reflected the periods of low soil moisture (Fensholt & Sandholt, 2003). When implemented using high temporal resolution data (15 min temporal resolution) from the SEVIRI instrument onboard MSG, SIWSI was found to co-vary with short term changes in vegetation water status (Fensholt, Huber, Proud, & Mbow, 2010a).

Timely information provided from EO data has been implemented in early warning systems (EWS) for averting food shortage and famine, e.g. the United States Agency for International Development (USAID) Famine Early Warning System (FEWSNET) and the United Nation's Food and Agricultural Organization (FAO) Global Information and Early Warning System (GIEWS). When using VIS/NIR based indices, canopy water status is assessed from chlorophyll content. However, chlorophyll content responds more slowly and less direct to plant water shortage, as compared to canopy water content. Direct assessment of the canopy water content based upon information from SWIR would potentially shorten the response time required for canopy water stress and drought detection in dryland areas. Currently, global EO-based NPP products using the Production Efficiency Model (PEM) approach are not able to sufficiently integrate short-term, EO-derived, information related to growth constraints (primarily water) in arid and semi-arid areas (Fensholt et al., 2006). If the SWIR sensitivity to canopy water content can be successfully implemented in EO-based monitoring, improvements in dryland productivity assessment could be foreseen.

Data from polar orbiting environmental satellites (POES) are largely influenced by daily variations in the sun-target-sensor geometry (Fensholt, Sandholt, Proud, Stisen, & Rasmussen, 2010b). These wavelength dependent variations (caused by different degrees of absorption/transmittance of a surface) are therefore affecting derived indices (Morton et al., 2014) and can ultimately mask the signal inherent to changes in canopy water content. (Fensholt, Huber, Proud, & Mbow, 2010a) explored the potential of SWIR based canopy water stress detection from geostationary MSG data (fixed viewing geometry) as compared to MODIS (Moderate Resolution Imaging Spectroradiometer) data (being a POES) and found higher usefulness of the geostationary signal. Short term variations of seasonally detrended daily SIWSI and NDVI anomalies, derived from the geostationary MSG data, have been compared to periods of limited plant available water for sites in the Sahel (Olsen et al., 2013). This was based on the hypothesis that anomalies would increase or decrease as a result of changed canopy water status during dry spells. SIWSI anomalies were shown to be better suited for this approach than NDVI anomalies. However, variations in anomalies during non-dry periods resulted in false dry period identifications, thereby making implementation of the method unsuited for robust drought detection on a per-pixel level.

Testing SIWSI index anomalies on a larger spatial scale has not yet been attempted despite: a) the importance of short-term detection of vegetation stress at the regional scale, and b) that previous studies have presented and supported the hypothesis, that short term variations in index anomalies hold information on changes in canopy water status (Fensholt, Huber, Proud, & Mbow, 2010a; Fensholt & Sandholt, 2003; Fensholt, Sandholt, Proud, Stisen, & Rasmussen, 2010b; Olsen et al., 2013). The purpose of this study is therefore to test this hypothesis by analyzing both NDVI and SIWSI derived from geostationary satellite imagery at a river basin scale (approximately 250,000 km^2). For this purpose NDVI is calculated from the SEVIRI channel 1 (0.6 μm — Red) and channel 2 (0.8 μm — NIR) and SIWSI is calculated from channel 2 and channel 3 (1.6 μm — SWIR). The indices are evaluated during both a well-watered and dry period during the 2008 growing season in the Senegal River Basin. Further, the indices are examined in different forms; both as regular index values and as seasonally detrended anomalies derived from seasonal curve fitting using the TIMESAT software (Jonsson & Eklundh, 2004). For comparison and evaluation, modeled actual evapotranspiration (ETa) from a semi-arid subset of the Senegal River basin area, estimated using a distributed hydrological model (MIKE SHE), is used together with the CPC-FEWS RFE2 gridded rainfall product.

2. Case area description

The Senegal River basin is located in West Africa and has a total drainage area of approximately 350,000 km^2. It covers parts of four countries; Guinea, Senegal, Mali, and Mauritania and is characterized by a strong rainfall and vegetation gradient, with little rainfall and vegetation in the north and increasingly dense vegetation and more annual rainfall towards the south (Fig. 1). The basin can be divided into sub-catchments, see (Stisen, Jensen, Sandholt, & Grimes, 2008), of which the semi-arid ones are of interest in this study and constitutes close to 250,000 km^2. The average annual rainfall for the sub-catchment shown in Fig. 1 is just below 500 mm/year, ranging from <200 mm/year in the north to >900 mm/year in the south. Maximum and minimum temperatures are around 40 °C and 17 °C respectively during the dry season (November to May) and 32 °C and 24 °C during the rainy season (June to October), but cooler close to the coast (weather-and-climate.com). The dominant soils types are arenosols, lithosols and regosols (FAO Harmonized World Soil Database — www.fao.org). The vegetation is predominantly natural and according to the USGS global Land Cover Classes (LCCs) savanna, grassland, shrubland, and barren or sparsely vegetated areas constitutes the majority of the area, with less than 6% identified as cropland (Table 1).

3. Data

3.1. Rain gauges

The rain gauge data are needed for assessing the uncertainties of gridded rainfall data in the case area. Within the Senegal River basin rain gauge data from 9 meteorological stations have been acquired from the NOAA Climate Data Online (CDO) facility http://www7.ncdc.noaa.gov/CDO/cdo (Table 2). Although more stations are present within the basin, many are without data for 2008.

3.2. CPC-FEWS Rainfall Estimation Algorithm version 2 (RFE2)

For this study a gridded rainfall product of high spatial and temporal resolution was needed, to facilitate the comparison with daily satellite data (NDVI and SIWSI) and modeled actual evapotranspiration. The Climate Prediction Center (CPC) Rainfall estimate product (Herman,

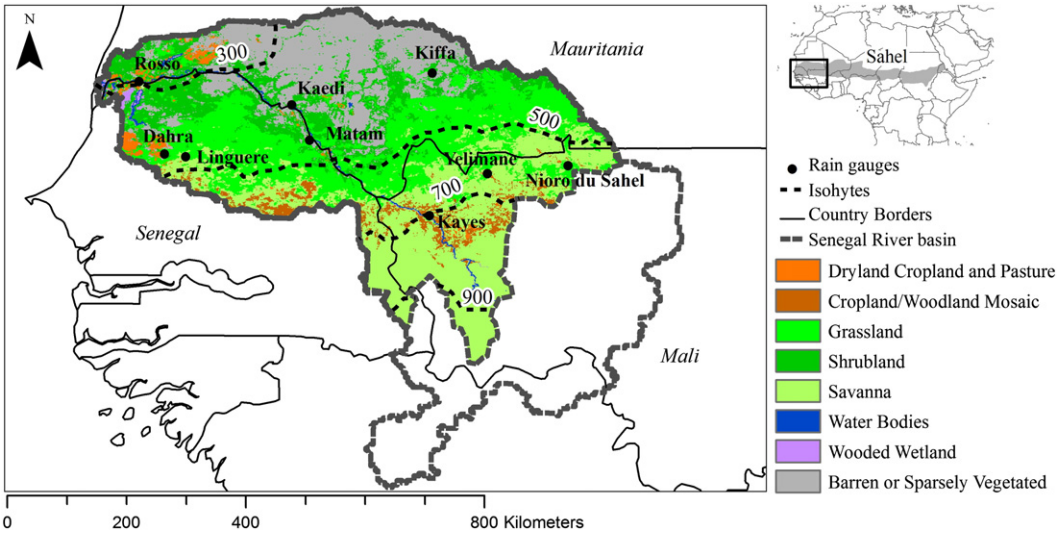

Fig. 1. The semi-arid sub-catchments of the Senegal River basin with USGS global land cover classes. The full basin is marked with dark gray line. 200 mm isohytes (hashed lines) from average rainfall for 2001 to 2013 calculated from NOAA RFE2 gridded rainfall product, and rain gauges (black dots).

Kumar, Arkin, & Kousky, 1997) version 2 (RFE2), has been found to perform acceptably for several African river basins (Thiemig, Rojas, Zambrano-Bigiarini, Levizzani, & De Roo, 2012) although with some difficulties for more complex terrain (Dinku, Chidzambwa, Ceccato, Connor, & Ropelewski, 2008). It is based on a combination of data sources including microwave, IR from geostationary satellites, and gauge data. With a spatial resolution of 0.1 degree lat/lon, daily estimates, and being available for 2000 and onwards, it fits the purpose of this study well.

3.3. MIKESHE modeled actual evapotranspiration (ETa)

Actual evapotranspiration estimates were derived using a distributed hydrological model set up using the MIKE SHE code (Abbott, Bathurst, Cunge, Oconnell, & Rasmussen, 1986) for the Senegal River basin. The model includes components for groundwater, unsaturated zone flow, evapotranspiration, overland flow and river routing. A modified version of the MIKE SHE code is utilized in this study, where groundwater flow (SZ) is represented by a series of interconnected linear reservoirs defined by storage capacities and residence times (Andersen, Refsgaard, & Jensen, 2001). Flow in the unsaturated zone (UZ) is assumed to be only vertical and gravity driven, which implies that upward flow in the unsaturated zone is neglected.

Actual evapotranspiration simulations are based on the formulation by (Kristensen & Jensen, 1975) accounting for interception, soil evaporation and plant transpiration. Interception is estimated as a function of leaf area index (LAI) and canopy storage capacity. The actual transpiration (E_{trans}) calculation is based on potential evapotranspiration (PET) corrected by three reduction functions f_1, f_2 and f_3 representing the dependency of transpiration on soil moisture in the root zone (f_1), vegetative cover (LAI) (f_2) and root depth and distribution (f_3).

Table 1
Distribution of case area land cover classes in percent.

Land cover class	Area (%)
Savanna	28.3
Grassland	27.2
Barren or sparsely vegetated	21.6
Shrubland	15.6
Cropland/woodland mosaic	3.5
Dryland cropland and pasture	2.1
Water bodies	1.2
Wooded wetland	0.5

The hydrological model has been setup and calibrated for the entire Senegal River Basin as described in (Stisen & Sandholt, 2010; Stisen et al., 2008). The horizontal discretization is 4 km × 4 km and within each grid the vertical unsaturated soil profile is discretized into computational layers of 5–50 cm. The model is driven by daily CPC-FEWS v2 precipitation data and monthly means PET data estimated from geostationary remote sensing (Stisen et al., 2008). The soil parameters are derived from the FAO soil map of the world while the land surface is parameterized using MODIS MCD15A2 8-day LAI product and estimates for root depth derived from the MODIS LAI.

The model has been calibrated against river discharge from six discharge stations as described in (Stisen & Sandholt, 2010; Stisen et al., 2008) using the shuffled complex evolution (SCE) algorithm (Duan, Sorooshian, & Gupta, 1992). The overall water balance is reasonable with 0–8% error. However, it's very difficult to quantify the uncertainty of the model simulated spatial and temporal patterns of ETa because no ground truth data exists that matches the temporal and spatial scale of the simulated maps. Although the model was originally setup for the entire Senegal River Basin, only simulations of actual evapotranspiration from the Northern and semi-arid part of the basin are utilized in this comparative study.

3.4. MSG SEVIRI

The SEVIRI instrument onboard the MSG geostationary platform provides observations every 15 min from its location at 0° longitude over the equator. The observations produced are at a 3 km sampling resolution at sub satellite point in 12 spectral channels, including a high resolution broadband visible channel with a 1 km spatial sampling distance (Schmetz et al., 2002). Level 1.5 MSG SEVIRI data are acquired in real time through the EUMETCast service, and an operational MSG SEVIRI processor has been built at the Department of Geosciences and Natural Resource Management, University of Copenhagen, to compute Earth surface reflectances. Atmospheric correction was performed using an improved version (Proud et al., 2010) of the SMAC algorithm (Rahman & Dedieu, 1994) using daily values of atmospheric water vapor, ozone and aerosols from the Level-3 MODIS Terra (MOD08_D3) and Aqua (MYD08_D3) Atmosphere Daily Global Products as inputs. MSG SEVIRI data are cloud-masked using both the cloud mask product (CLMK) from MSG Meteorological Products Extraction Facility (MPEF) (Lutz, 2009) and the CMa product produced using software from the satellite applications facility in support of nowcasting and very short-range weather forecasting.

Table 2
Rain gauges in the Senegal River Basin with summed measurements from 2008 and land cover class from the USGS EROS Land Cover dataset version 2.0.

Station	Country	Latitude	Longitude	2008 rainfall, gauge (mm)	Land cover
Kayes/Dag-Dag	Mali	14.48	−11.44	428	Savanna
Yelimane	Mali	15.12	−10.57	136	Savanna
Nioro du Sahel	Mali	15.23	−9.35	349	Grassland
Linguere	Senegal	15.37	−15.12	479	Grassland
Dahra	Senegal	15.41	−15.44	317	Grassland
Matam	Senegal	15.62	−13.25	423	Barren or sparsely vegetated
Kaedi	Mauritania	16.15	−13.52	230	Barren or sparsely vegetated
Rosso	Mauritania	16.50	−15.82	272	Dryland cropland and pasture
Kiffa	Mauritania	16.63	−11.4	325	Barren or sparsely vegetated

The atmospherically corrected and cloud masked land surface reflectances from SEVIRI are affected by the changing illumination and viewing geometry between sun, target, and sensor (Fensholt, Sandholt, Proud, Stisen, & Rasmussen, 2010b). This is minimized by using a Bidirectional Reflectance Distribution Function (BRDF) to describe the angular dependency, making it possible to produce reflectances normalized to a common set of solar and viewing angles. A Nadir view BRDF Adjusted Reflectance (NBAR) product has been created on a daily basis for channel 1 (VIS 0.6 μm), channel 2 (NIR 0.8 μm), and channel 3 (SWIR 1.6 μm), by using a modified version of the algorithm used for the MODIS NBAR product (Ju, Roy, Shuai, & Schaaf, 2010; Proud et al., 2014; Schaaf et al., 2002). The NBAR product is created using data from the given day, as well as up to four preceding days, providing a maximum of 5 days of observations as input. The product retains sensitivity to short term variations of surface reflectance, while the chance of retrieving sufficient cloud free observations for a successful inversion increases by combining several days of data (Proud et al., 2014).

4. Methods

The archive of rainfall RFE2 data was studied for the Senegal River basin to find growing season periods characterized by substantial water shortage at the catchment scale. In 2008 a large part of the river basin experienced a dry period during the growing season between DOY 253 and 262, as identified in a previous study for a limited area around the Dahra test site (Fensholt, Huber, Proud, & Mbow, 2010a) and by both gauge and RFE2 rainfall estimates. This period is well suited to examine the performance of NDVI and SIWSI for limited water availability on a short time scale.

4.1. Rainfall and actual evapotranspiration

Daily RFE2 estimates were temporally aggregated for the 10-day period (DOY 253–262) because of the uncertainty of the RFE2 estimates at a daily time scale. To put this into growing season context four preceding 10-day periods of RFE2 were also summed as well as the one following 10-day period. Aggregating on a 10-day basis serves to increase the correlation between gauge (Table 2) and RFE2 estimates from r = 0.12 (daily estimates) to r = 0.79 (10-day sums, see Fig. 2), and alleviates the inconsistencies on both timing and amount of rainfall for the two data sets. As the modeled actual evapotranspiration (ETa) is driven by RFE2 estimates, amongst other parameters, ETa is averaged on 10-day basis for easier comparison.

4.2. Index calculation and seasonal detrending

Using the SEVIRI NBARs, NDVI is calculated from daily red and NIR reflectances (Eq. 1), and SIWSI is calculated from daily NIR and SWIR reflectances (Eq. 2). For seasonal detrending of the indices, suitable fittings of growing season trends are derived using the TIMESAT software. For this purpose SIWSI is inverted by multiplying by −1 (Eq. 2). This is necessary as growing seasons will normally appear as decreasing values in a SIWSI time series, and TIMESAT is based on the assumption that growing seasons will be distinguishable by increased values.

$$\mathrm{NDVI} = \frac{\mathrm{NIR} - \mathrm{red}}{\mathrm{NIR} + \mathrm{red}} \quad (1)$$

$$\mathrm{SIWSI}_{\mathrm{inv}} = -1 * \frac{\mathrm{SWIR} - \mathrm{NIR}}{\mathrm{SWIR} + \mathrm{NIR}} \quad (2)$$

Furthermore, TIMESAT does not handle data with many gaps well. Therefore pixels with no values in NDVI and SIWSI imagery have been filled by 2d spline interpolation (see (D'Errico, 2004) for the full algorithm). Due to the large number of observations going into the NBAR product, the vast majority of gaps are spatially quite small. The full year of NDVI and SIWSI 2008 imagery is used as input in TIMESAT. Previous implementation of fitting functions to the distinct Sahelian growing season seen in daily vegetation and vegetation water sensitive indices suggests the use of Savitsky–Golay (SG) filtering with 30 day windows (Olsen et al., 2013), which is also implemented in this study. The number of time steps used for SG fitting determines how detailed the fitting is. The larger window used, the less detailed and more smoothed fitting. A 30 day window used here is the largest window that can be applied, which still retains accurate estimates of onset and end of growing season. Larger windows will result in a flatter curve with too early onset and too late end estimates. Examples of NDVI and SIWSI time series and Savitsky–Golay fittings for the Linguere site (Fig. 1) are shown in Fig. 3A.

By subtracting the Savitsky–Golay fitted values from the NDVI and $\mathrm{SIWSI}_{\mathrm{inv}}$ time series, daily anomalies are produced (see examples in Fig. 3B and C). While the fitted values represent the general seasonal trend for each pixel, the anomalies contain information on short term variations as well as noise. With water as the primary constraint for

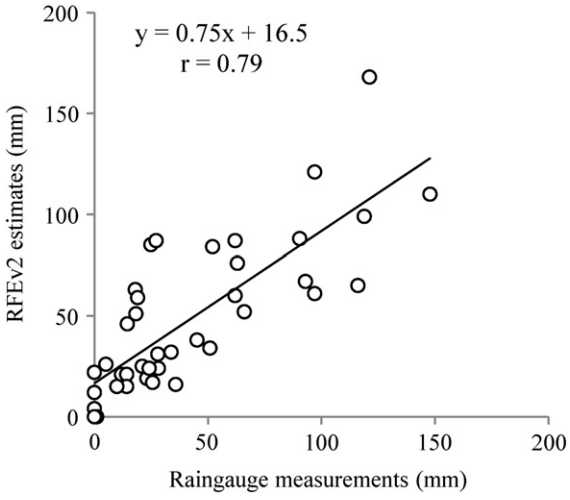

Fig. 2. Comparison of 10-day summed rainfall, x-axis: gauges within the Senegal River Basin (Table 2, n = 9) in 2008, y-axis: values of RFEv2 rainfall.

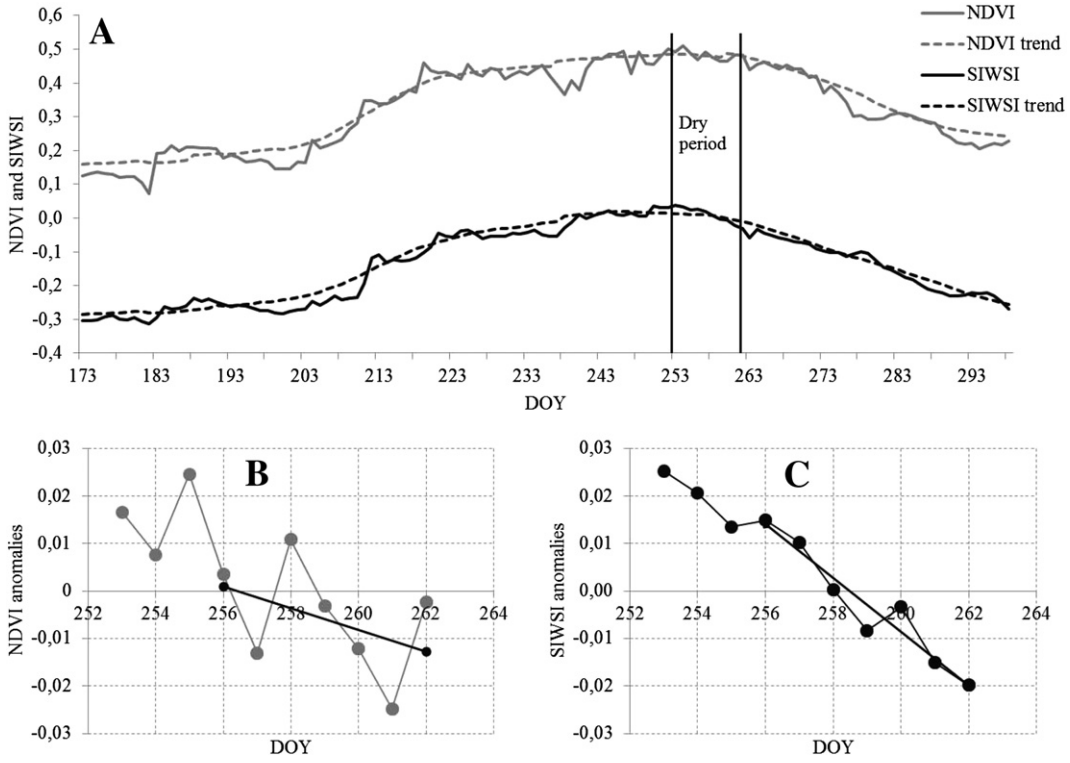

Fig. 3. A) Example of SEVIRI NDVI and SIWSI time series for the pixel overlapping the Linguere site. The dashed lines represent trends derived using TIMESAT Savitsky–Golay fittings. Marked in vertical lines are the 10-day period (DOY 253–262) identified as dry for large parts of the catchment area. B) NDVI anomalies for the 10-day dry period, with 7 day linear trend fitted. C) SIWSI anomalies and 7 day linear trend.

vegetation growth in Sahel, it can be hypothesized that short term variations in canopy water sensitive indices are related to changes in canopy water status (Fensholt & Sandholt, 2003; Fensholt, Huber, Proud, & Mbow, 2010a; Olsen et al., 2013).

The sandy soils predominant in the area can be expected to drain to about field capacity after a few days without rainfall (Olsen et al., 2013). Furthermore, a study by (Proud & Rasmussen, 2010) mentions that farmers in the Sahel expects more than 5 consecutive dry days in the growing season to potentially influence crop growth negatively. Therefore a period of 7 days is selected as a reasonable length for assessing the short term evolution of the daily anomalies. 7-day periods can also easily be examined in relation to the 10-day summed RFE2 and 10-day averaged ETa by comparing with the 7 last days of anomalies in a RFE2 or ETa period. To quantify the temporal evolution, linear trends are fitted to the anomalies (examples for Linguere pixel in Fig. 3B and C) and the first day fitted value is subtracted from the seventh day fitted value. The fitted trends are assessed by calculating correlation coefficients (r) and p-values. The p-values take into account the relatively few observation points (7) and a 95% significance criteria ($p < 0.05$) is applied. Spatial coherence of significant anomaly trends (e.g. meaningful or "salt-n-pepper") will also indicate whether or not the results are reliable.

5. Results

The results in this section are presented on three different time intervals. First rainfall is summed on 10-day basis and ETa is averaged on 10-day basis. Secondly NDVI and SIWSI are presented as daily imagery, and thirdly, detrended daily anomalies of both NDVI and SIWSI are presented as changes over seven days.

5.1. Growing season rainfall 2008

The summed rainfall is shown for six 10-day periods covering the mid-growing season of 2008 and the general tendency of a north/south gradient with larger amounts of rainfall in the south is observed (Fig. 4). The mean basin rainfall for the first two periods and the last period is of similar magnitude (31, 29, and 39 mm), while the two middle periods, DOY 233–242 and 243–252, were wetter and received 80 and 61 mm respectively. The DOY 253–262 period is the driest during the growing season with a spatial mean of only 16 mm, and parts of the western half of the river basin received no rainfall at all during the 10-days.

The rainfall isohytes show how savanna areas receive the most rainfall, followed by grassland and with shrubland and barren or sparsely vegetated areas receiving the least (Fig. 1). For the wettest period (DOY 233–242) the relative difference between received rainfall in northern and southern parts of the river basin is small, with shrubland (driest) receiving 68% of the savanna rainfall. For the driest period (DOY 253–262) the difference is larger and the LCC barren or sparsely vegetated receives only 37% of savanna rainfall.

5.2. Growing season evapotranspiration 2008

The modeled estimates of ETa are shown in (Fig. 5) as averages of 10-day values to better facilitate comparison with rainfall. ETa follows the north/south gradient, but also reflects the spatio-temporal pattern of rainfall. The sub-catchment mean values (noted in Fig. 5) are lowest for the 223–232 period and not for the 253–262 period, where the least rainfall is recorded. The average spatial correlation between the 10-day periods of ETa and rainfall is modest ($r = 0.55$), while stronger between the ETa 10-day averages and the daily indices for the end days of the 10-day periods (mean $r = 0.73$ for both NDVI and SIWSI).

5.3. Daily NDVI and SIWSI for 2008

Examples of daily SEVIRI NDVI and SIWSI imagery for the Senegal River basin (DOY 262, 2008) are shown in (Fig. 6A) and (B). Values for both indices increase from north to south, confirming vegetation sensitivity to the region's pronounced rainfall gradient. A high spatial

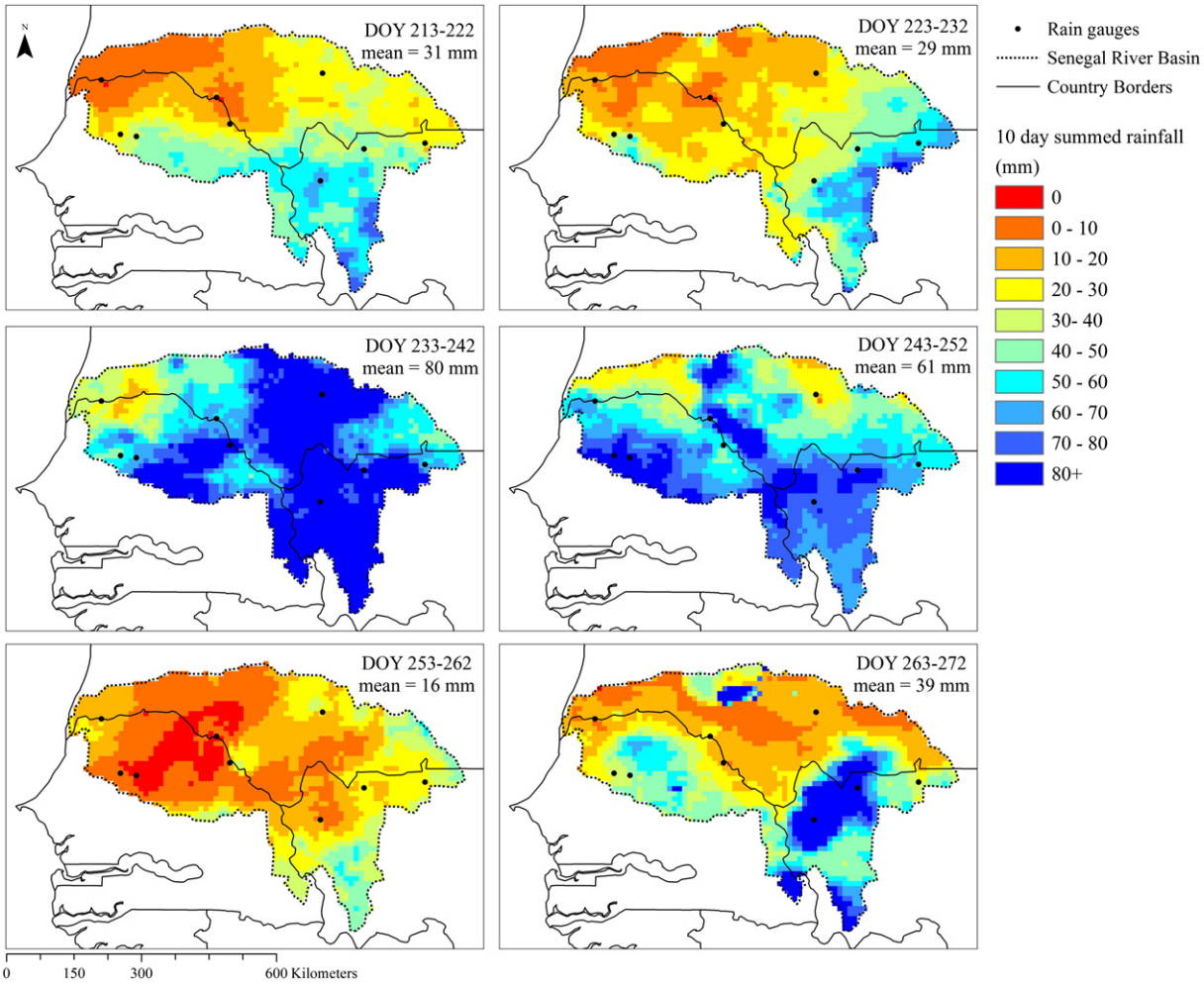

Fig. 4. Summed rainfall for 10-day periods in mid-growing season 2008, derived from RFEv2 daily gridded rainfall product. The spatial mean is noted for each period.

correlation between the two indices is found ($r = 0.85$), but when comparing the indices for the individual LCCs the range of values are reduced and the correlation coefficients is lower, especially for drier and less vegetated areas, with r values of 0.81 for savanna, 0.75 for grassland, 0.51 for shrubland, and 0.42 for barren or sparsely vegetated.

The mean values and standard deviations of daily NDVI and daily SIWSI (Table 3) are shown for six selected days (the days at the end of the 10-day periods for which gridded rainfall is summed) and for the four dominant LCC, as well as for the full river basin. The low average annual rainfall (Fig. 1) and short growing season of the barren or sparsely vegetated area in the north of the river basin (Table 3) means that the values of NDVI and SIWSI for DOY 222 can be used as an approximation of pre-growing season bare soil values. For NDVI this value is 0.17 and for SIWSI it is −0.25. Increase in mean values for shrubland and barren/sparsely vegetated LCC are only observed for DOY 242–262, whereas the higher values of both indices for savanna and grassland shows growing season onset before DOY 222 for the southern parts of the river basin.

For both indices mean values and standard deviations are highest for savanna and lowest for the barren or sparsely vegetated areas, with grassland and shrubland in between. On average, the NDVI standard deviations are 0.015 higher than SIWSI (for all LCC and all 6 days). The mean NDVI values of savanna and grassland are observed to decrease from DOY 222 to DOY 232 with 0.07 and 0.05 respectively (Table 3), while there were little change in values for the shrubland and barren or sparsely vegetated LCC (0.02 and 0.01). Later in the season, after the dry period (DOY 253–262), the daily NDVI values decrease for all LCC between 0.03 and 0.06 and keep decreasing from DOY 262 to 272, except for savanna, which rises again. While these variations are observed in NDVI, the SIWSI daily values for all LCC increase continually until DOY 252 and then decrease again (Table 3). For both NDVI and SIWSI there are no consistent patterns to be observed in the temporal variation of the standard deviations.

5.4. Detrended indices

The NDVI and SIWSI anomalies are presented here as the change over 7 days derived from linear trends (Fig. 7A and B). The correlation coefficients of the per-pixel linear trend of 7 day anomaly values are shown in (Fig. 7C and D). Pixels with $-0.76 > r > 0.76$ are found significant ($p < 0.05$) and pixels with $-0.88 > r > 0.88$ are found highly significant ($p < 0.01$). For both NDVI and SIWSI anomalies, there are spatially coherent areas with significant trends.

The NDVI and SIWSI changes in anomalies for the 7 days up to DOY 222, 262, and 272 show similarities in some general spatial patterns. On DOY 222, negative trends are seen for both sets of anomalies for the westernmost grassland and shrubland between the Linguere and Rosso sites (Fig. 1), while an area of positive trends are observed east-southeast of Linguere. The index anomalies are not similar for the southern savanna areas, as SIWSI anomalies show negative trends for most of the area, while NDVI anomalies show both positive and negative trends.

For the period up to and including DOY 232, anomalies in the western half of the catchment have similar general patterns. However, the

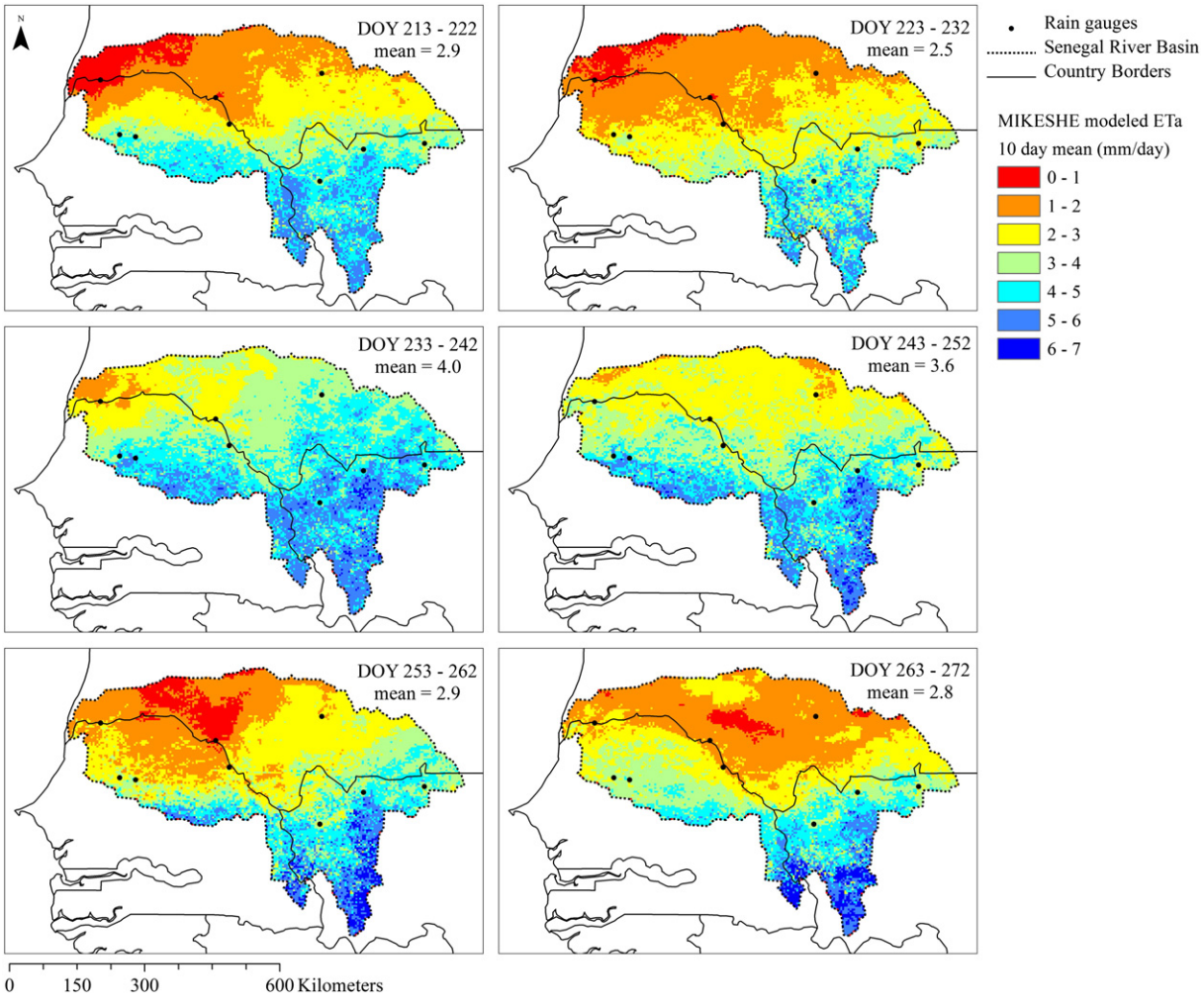

Fig. 5. 10-day averages of MIKESHE modeled actual evapotranspiration (ETa) in mm/day for the Senegal River basin during mid-growing season of 2008.

eastern half, including the savanna-dominated southern tail of the catchment, has mostly opposite trends; negative for NDVI anomalies and positive for SIWSI. For the periods up to DOY 242 and 252 the anomalies from the two indices are unrelated, and far more pixels with significant increases are observed for SIWSI anomalies than for NDVI anomalies. These are the two periods of high average rainfall in the river basin.

The spatial patterns of anomalies up to DOY 262 and 272 are in better agreement for savanna, grassland and shrubland. For the barren or sparsely vegetated northern areas, patches of both increasing and decreasing SIWSI anomalies trends are observed, while NDVI anomalies almost unanimously have decreasing trends. However, while many pixels have significant trends the absolute change in anomalies are small. This is especially true for shrubland and barren or sparsely vegetated areas, and spatially most extensive on DOY 272. Areas with less vegetation will have small seasonal amplitude in per pixel time series of vegetation indices.

5.5. ETa and index anomalies

Scatterplots of ETa 10-day means aggregated for the four dominant LCCs and the linear fitted change in index anomlies are shown for NDVI anomalies in Fig. 8A and SIWSI anomalies in Fig. 8B. The values are derived with 10-day time intervals, starting at DOY 192 and ending on DOY 272. The 7 day change in index anomalies aggregated for LCCs range from −0.082 to 0.092 for NDVI (range of 0.174), with largest negative and positive change found for savanna. For SIWSI the range is from −0.041 to 0.034 (range of 0.075) with largest negative change found for savanna and largest positive change found for shrubland. Except for the relation between shrubland modeled ETa and NDVI anomalies, all relations are statistically significant ($p < 0.05$), despite the limited number of observation points. For all four LCCs the correlation coefficients are higher between SIWSI anomalies (Fig. 8B) and ETa, than for NDVI anomalies (Fig. 8A) and ETa.

6. Discussion

An evaluation of NDVI and SIWSI sensitivity to canopy water status at the catchment scale inevitably includes satellite based rainfall estimates, especially for an area of limited gauge data availability and high spatial rainfall variability. The comparison between rain gauges and RFE2 within the river basin for the 2008 growing season showed that summing on 10-day basis is necessary to attain a good agreement (Fig. 2). As it is considered challenging to produce reliable gridded rainfall estimates, especially with high temporal and spatial resolutions (Dinku et al., 2008; Pierre et al., 2011; Stisen & Sandholt, 2010) and data from weather stations may also contain large uncertainties (Zhao, Running, & Nemani, 2006) it was decided to conduct the index evaluation on the basis of 10-day periods even though the index values could be applied on daily time scales. Although lacking the information on specific rainfall events, the 10-day summed estimates are still sufficient to describe the general seasonal distribution of rainfall and are considered more reliable for index evaluation purposes. The general rainfall gradient (Fig. 4) is clearly observed on an intra-seasonal timescale in

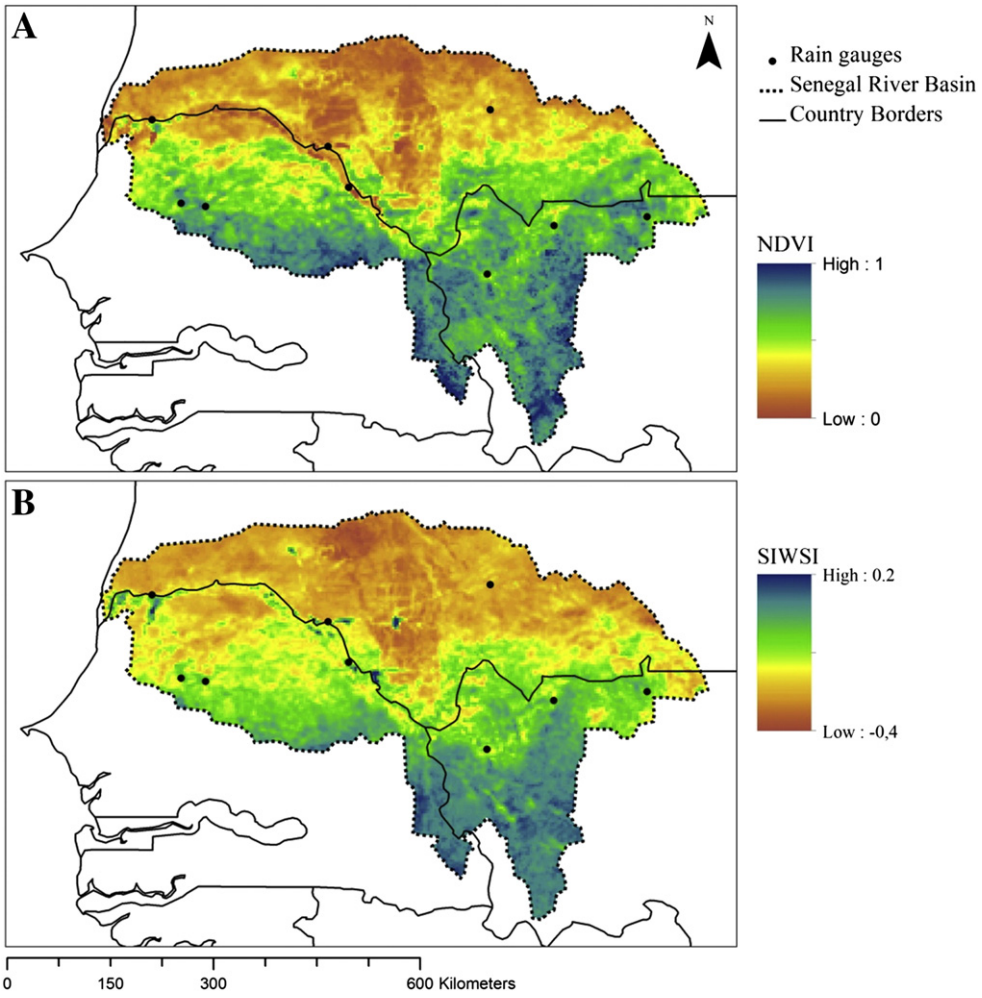

Fig. 6. A–B: Examples of daily NDVI (A) and SIWSI (B) Indices calculated from SEVIRI NBAR product for the Senegal River basin on DOY 262, 2008.

Table 3
Daily NDVI and SIWSI mean values and standard deviations for the semi-arid subset of the Senegal River basin (All) and divided by the four dominant USGS land cover classes (savanna, grassland, shrubland, and barren or sparsely vegetated).

	DOY	All	Savanna	Grassland	Shrubland	Barren
NDVI mean values	222	0.32	0.48	0.33	0.21	0.17
	232	0.28	0.41	0.28	0.19	0.16
	242	0.33	0.53	0.32	0.20	0.18
	252	0.38	0.54	0.39	0.27	0.23
	262	0.34	0.48	0.36	0.24	0.18
	272	0.34	0.53	0.33	0.22	0.16
NDVI standard deviations	222	0.32	0.48	0.33	0.21	0.17
	232	0.28	0.41	0.28	0.19	0.16
	242	0.33	0.53	0.32	0.20	0.18
	252	0.38	0.54	0.39	0.27	0.23
	262	0.34	0.48	0.36	0.24	0.18
	272	0.34	0.53	0.33	0.22	0.16
SIWSI mean values	222	−0.132	0.024	−0.15	−0.24	−0.25
	232	−0.113	0.039	−0.14	−0.21	−0.23
	242	−0.078	0.075	−0.10	−0.18	−0.20
	252	−0.073	0.075	−0.09	−0.17	−0.20
	262	−0.103	0.033	−0.12	−0.19	−0.22
	272	−0.129	0.015	−0.16	−0.21	−0.24
SIWSI standard deviations	222	0.137	0.090	0.084	0.058	0.057
	232	0.137	0.103	0.075	0.060	0.058
	242	0.142	0.107	0.085	0.073	0.067
	252	0.143	0.104	0.086	0.075	0.076
	262	0.130	0.095	0.077	0.069	0.069
	272	0.134	0.120	0.071	0.058	0.062

2008. However, the difference in rainfall is small during the wettest period between savanna and barren or sparsely vegetated LCCs. This indicates that the rainfall gradient is less pronounced during the wettest periods because of the northern position of the ITCZ (Intertropical Convergence Zone).

The MIKESHE modeled ETa includes information on both daily and seasonal time scales, reflecting rainfall and vegetation water status, as well as the general vegetation gradient over the growing season. While a modest spatial relation between rainfall and evapotranspiration is found ($r = 0.55$), and the two periods of high rainfall are clearly reflected in the mean ETa (Fig. 5), it is noticeable that stronger relations are found between ETa and both the NDVI and SIWSI ($r = 0.73$ for both), again pointing to the interaction between rainfall and vegetation on longer time scales. This can be interpreted as ETa being primarily location determined, and thus reflecting the rainfall/vegetation gradient first and short term variations in canopy water status second.

The spatial coherent patterns of seven day changes in NDVI and SIWSI index anomalies, together with the significant linear trends of these changes (Fig. 7), show that much of the temporal variation in anomalies does contain information about canopy water status with an acceptable signal/noise ratio. It is worth noting that TIMESATs SG filtering used for detrending is quite sensitive to the algorithm settings. In particular the window size, i.e. the number of time steps used for deriving each value of the seasonal trend. The choice of applying a large window in this study (30 days) results in relatively smoothed fittings (as seen in Fig. 3), which have limited sensitivity to quick variations in index time series. This is good for retrieving anomalies that reflects

short term changes. However, the SG filter is sensitive to longer changes during a growing season, and prolonged droughts over several weeks will be reflected in the derived seasonal trend. Hence, canopy water stress information at longer time scales will not be found in the anomalies. The use of SG filtering is also discussed in (Jonsson & Eklundh, 2004; Olsen et al., 2013).

By seasonal detrending of NDVI and SIWSI most of the location dependency is removed. Naturally, a pixels range of index values over a growing season still determines the limits of the potential size of anomalies.

Also, for areas with less vegetation the satellite signal in red/NIR/SWIR used as input for the indices are likely more affected by soil background. However, compared to absolute values of both rainfall and ETa the north/south gradient of the river basin has little influence and the magnitude of anomalies is similar for all LCCs. The exception being NDVI anomalies for pixels designated as savanna (Fig. 8A). This can be a large advantage when estimating the status of vegetation, as a multi-annual time series of imagery are not needed to determine what the norm is, and whether a season deviates from the norm of other years. This is especially true in the Sahel, where areas dominated by annual plant species are spatially extensive (Breman & Dewit, 1983; Elberse & Breman, 1989), and annual plant species composition may vary noticeably on year-to-year basis. This was shown in a study based on detailed in situ measurements of NDVI, soil moisture, biomass, and species composition for the Dahra test site (Mbow, Fensholt, Rasmussen, & Diop, 2013). As the seasonal evolution of time series of vegetation indices can change depending on species composition, a multi-year average timeline can be a somewhat artificial result of combining time lines from common but varying species. How the vegetation reacts to periods of plentiful or limited plant water availability may also vary inter-annually, as species have different germination characteristics and drought resilience (Elberse & Breman, 1989, 1990).

By examining seasonally detrended anomalies from both NDVI and SIWSI, this study shows, as confirmed by (Fensholt & Sandholt, 2003; Fensholt, Huber, Proud, & Mbow, 2010a; Olsen et al., 2013), that index anomalies from especially SIWSI, hold information on short term variations in canopy water status that can be separated from the seasonality and noise related to sun-target-sensor geometry. However, two challenges to meaningful implementation of SIWSI anomalies for water stress detection exist: first, the need for seasonal detrending to retrieve daily index anomalies prevents implementation of the method in near-real time, and secondly the per pixel relation between anomalies and periods of limited plant available water was found insufficiently robust for drought monitoring (Olsen et al., 2013). However, many applications of indices based on annual time series, such as NPP modeling from annual or seasonal integrated NDVI (Fensholt et al., 2006; Prince, 1991a) and analysis of phenology, may still benefit from the added sensitivity to short term stress from the use of geostationary NIR/SWIR.

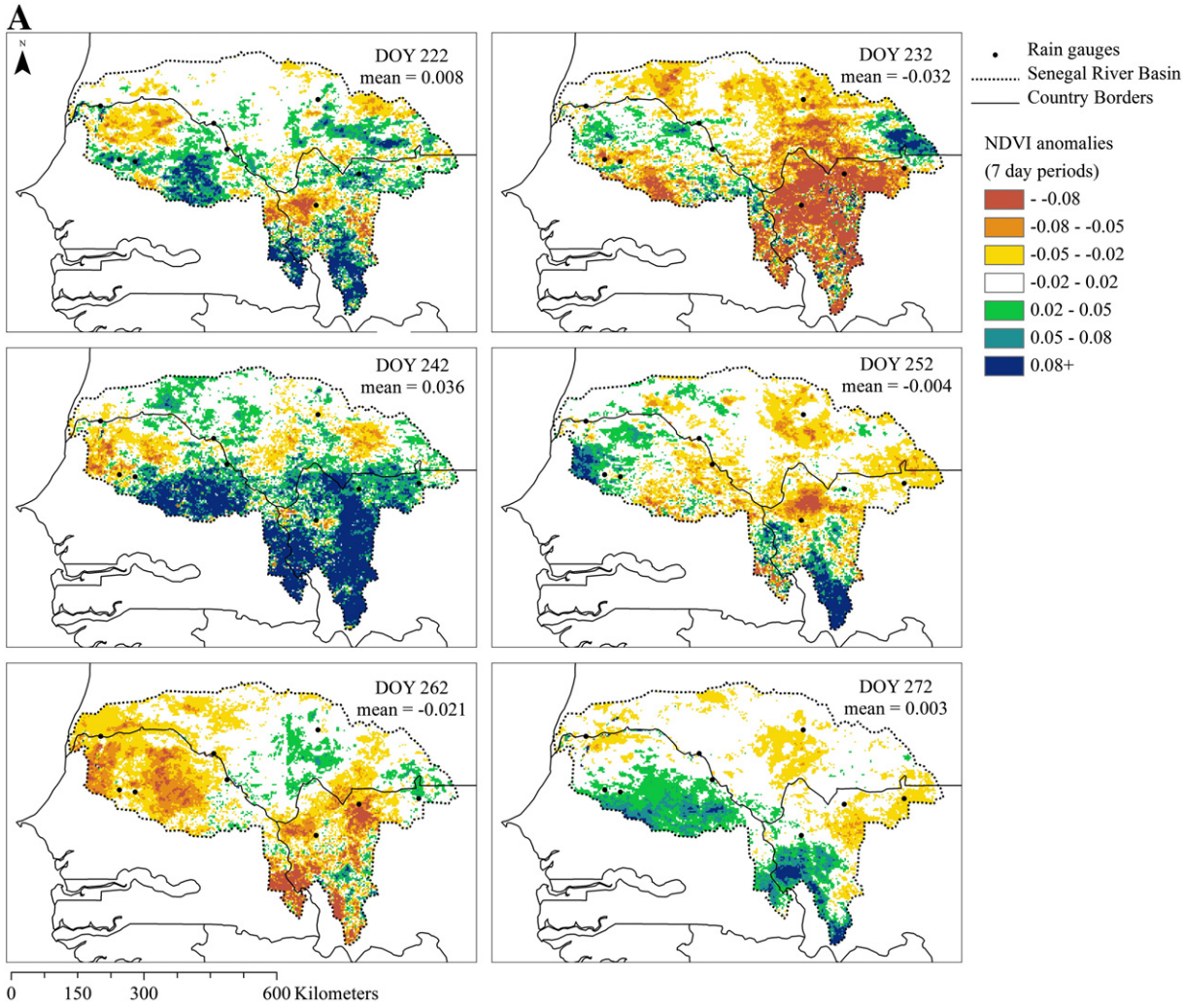

Fig. 7. A: Change in NDVI anomalies on 7 day basis, derived as the difference between end and start values of linear fittings of 7 consecutive anomaly values, from the days up to – and including – the DOY noted in each map frame. B: Change in SIWSI anomalies on 7 day basis, derived as the difference between end and start values of linear fittings of 7 consecutive anomaly values, from the days up to – and including – the DOY noted in each map frame. C: Correlation coefficients (r) for linear trends of 7 days NDVI anomalies. Values of $r > 0.76$ equal p values < 0.05 (two-tailed). D: Correlation coefficients (r) for linear trends of 7 days SIWSI anomalies. Values of $r > 0.76$ equal p values < 0.05 (two-tailed).

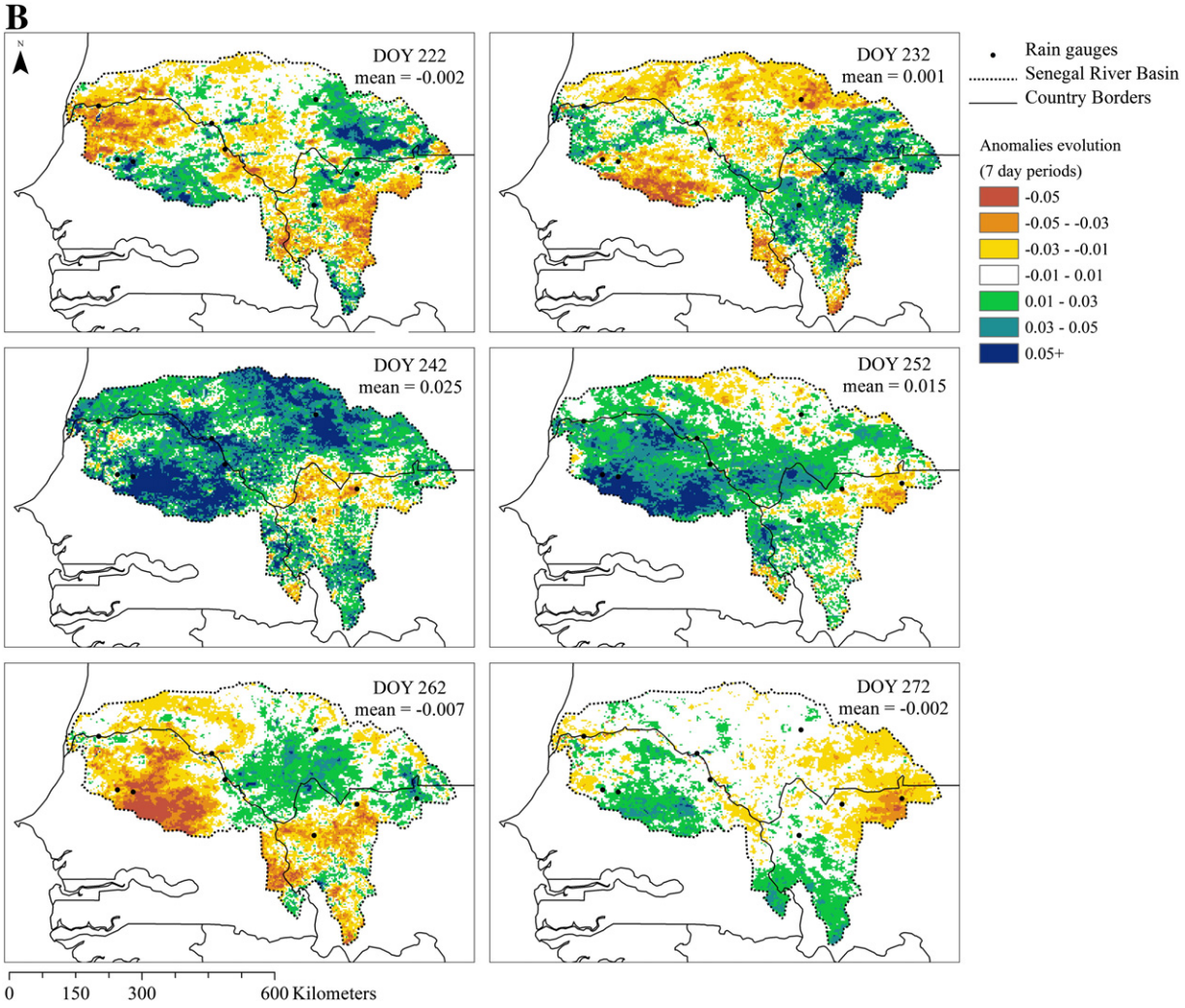

Fig. 7 (*continued*).

Especially in areas where vegetation growth is water restricted this could improve NPP modeling performance. The spatial coherent patterns of significant anomaly trends presented in this study suggest that the second issue may be addressed by spatial aggregation. As presented in Fig. 8, the 7 day fitted changes aggregated on basis of the four dominant LCCs within the river basin are significantly related to modeled ETa, and when compared to 10-day rainfall for each LCC the positive changes in anomaly values are noticeable for the two wet periods in the mid-growing season. In (Olsen et al., 2013) where NDVI and SIWSI anomalies were first examined for information on canopy water stress on a point/pixel basis for three sites in the Sahel, the focus was entirely on how periods of limited plant available water was reflected in short term variations in the signal. However, the positive trends in SIWSI anomalies during the wet period from DOY 233 to DOY 252 suggest that the influence of well watered periods is also captured in the short term changes in anomalies, when following less wet periods. This study further confirms the conclusion that SIWSI anomalies are more strongly related to short term variation in vegetation water status, as compared to NDVI (Fig. 8).

The very high temporal resolution of observations from the SEVIRI instrument onboard the geostationary MSG platform is important, as it allows for a sufficient high frequency of observations to create a robust daily NBAR product. Without a high quality daily product, the hypothesis that index anomalies capture short term variations in canopy water status could not be confirmed. This is also considered in the findings of (Fensholt, Huber, Proud, & Mbow, 2010a), where daily SIWSI from both the SEVIRI (geostationary) and MODIS (polar orbiting) sensors where compared, and covariation with surface layer soil moisture was only found between the SEVIRI based SIWSI and moisture measurements. In an earlier study however, SIWSI based on daily MODIS observations was found strongly related to daily estimates of soil moisture in northern Senegal in 2001. Although the same study concluded that for the following, and much dryer year, this could not be confirmed. It was argued that the severe dryness of the 2002 growing season limited vegetation growth to an extent, where the vegetation cover was insufficient to provide information on the canopy water content (Fensholt & Sandholt, 2003). The low spatial correlations found between NDVI and SIWSI for areas categorized as barren or sparsely vegetated (according to the USGS LCCs) in this study also indicates that sparse vegetation dampens the signal sensitivity to rapid changes in canopy water status. Still, the SIWSI anomalies observed in the northern and less vegetated parts of the Senegal River basin have statistically significant positive trends in the wet 10-day period of DOY 233–242, whereas this is not the case for NDVI anomalies for the same period and area.

7. Conclusions

In this study we evaluated the two indices Normalized Difference Vegetation Index (NDVI) and the Shortwave Infrared Water Stress Index (SIWSI) derived from the Spinning Enhanced Visible and Infrared Imager (SEVIRI) onboard the geostationary Meteosat Second Generation

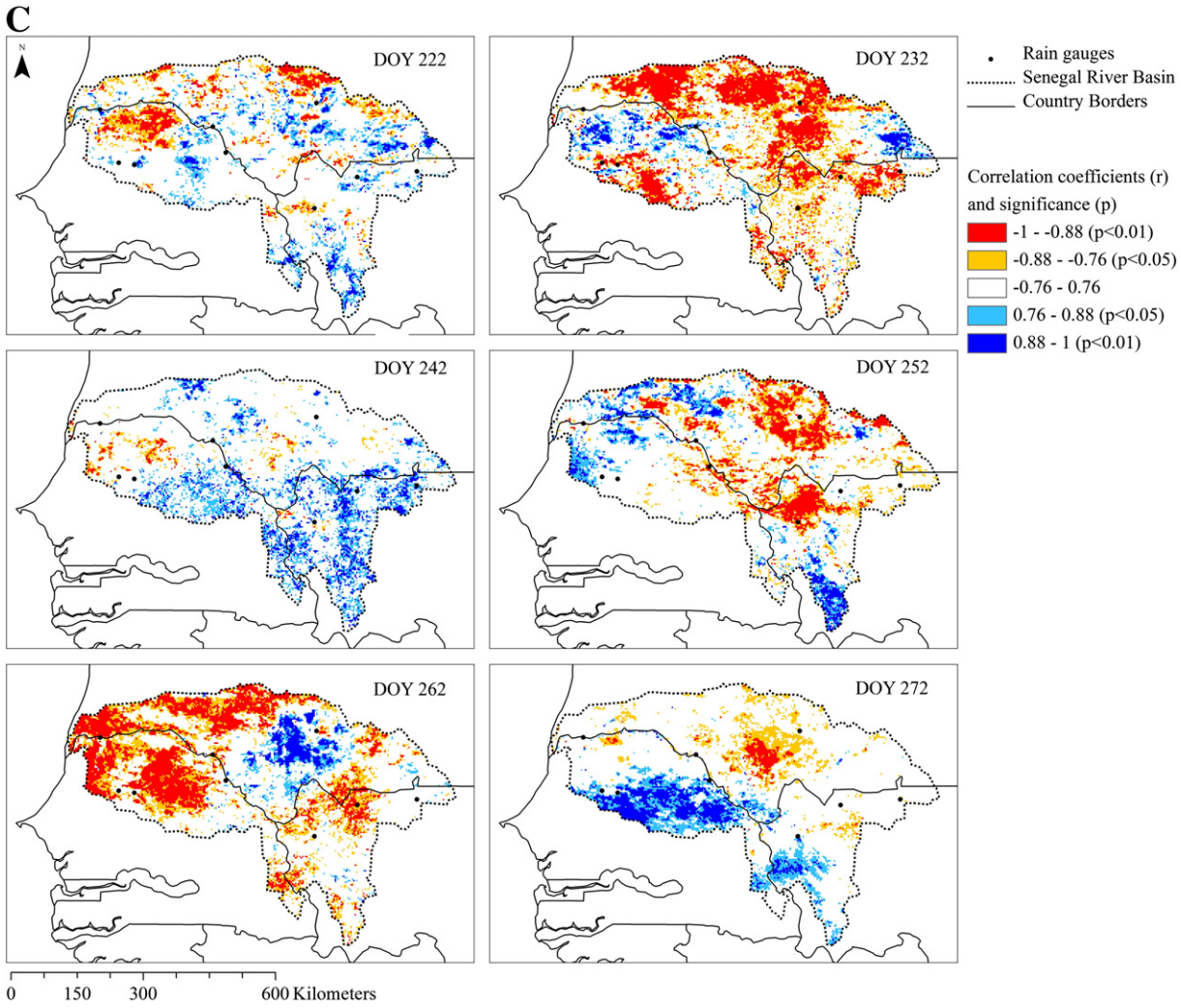

Fig. 7 (*continued*).

(MSG) platform. The main focus is on daily anomalies derived from seasonally detrended time series from the 2008 growing season in the semi-arid sub-catchment of the Senegal River basin.

The non-detrended daily NDVI and SIWSI indices were found spatially highly correlated to 10-day mean of MIKE SHE modeled actual evapotranspiration (ETa) with average $r = 0.73$, whereas 10-day summed rainfall estimates from RFE2 had a more modest correlation to ETa ($r = 0.55$), thereby showing how the pronounced north/south vegetation gradient in the river catchment, depending on long term rainfall patterns, is a more important factor for evapotranspiration than short term variations in rainfall.

The hypothesis that short term evolution of index anomalies are related to vegetation water status was tested both spatially and temporally using the gridded rainfall estimates (RFE2) product and modeled ETa. For SIWSI moderate to strong coefficients of determination was found between modeled actual evapotranspiration averaged over 10-days and short term variations in seasonally detrended daily anomalies (change assessed for periods of seven days), when anomaly variations were aggregated by Land Cover Classes (LCCs), with R^2 values of 0.65 for savanna, 0.60 for grassland, 0.72 for shrubland, and 0.58 for barren or sparsely vegetated areas. This is consistently higher than for the same method applied to NDVI anomalies (R^2 values found are 0.57 for savanna, 0.50 for grassland, 0.32 for shrubland, and 0.57 for barren or sparsely vegetated areas).

The combination of the SWIR sensitivity to canopy water content and the use of a daily Nadir view BRDF Adjusted Reflectance (NBAR) product created from geostationary MSG SEVIRI observations, allows for derivation of daily index anomalies holding information on short term changes in canopy water status. Therefore the approach of detrending NIR/SWIR based indices and spatially aggregating the anomalies do offer the opportunity of improved detection of intra-seasonal stress. This is also applicable in otherwise well-watered years for semi-arid regions where vegetation growth is primarily water restricted. However, quite coarse spatial aggregation, in this case based on USGS LCCs, is found necessary for a significant analysis outcome. This regional scale study adds an important dimension by showing clear and spatially coherent pattens of significant anomaly trends. Thereby underlining the reliability of the results and adding to existing knowledge from point-pixel based studies of SIWSI and NDVI in the context of Sahelian vegetation (Fensholt & Sandholt, 2003; Fensholt, Huber, Proud, & Mbow, 2010a; Olsen et al., 2013). It supports that intra-seasonal variations in canopy water status can be derived from SIWSI anomalies at the regional scale. Future research should test the applicability of such information to improve regional scale NPP modeling for semi-arid areas as suggested in (Fensholt et al., 2006). How to implement short term variations in SIWSI in a near real-time context, for potential implementation in Famine Early Warning Systems (FEWS), should also be studied further, as this is not currently feasible due to

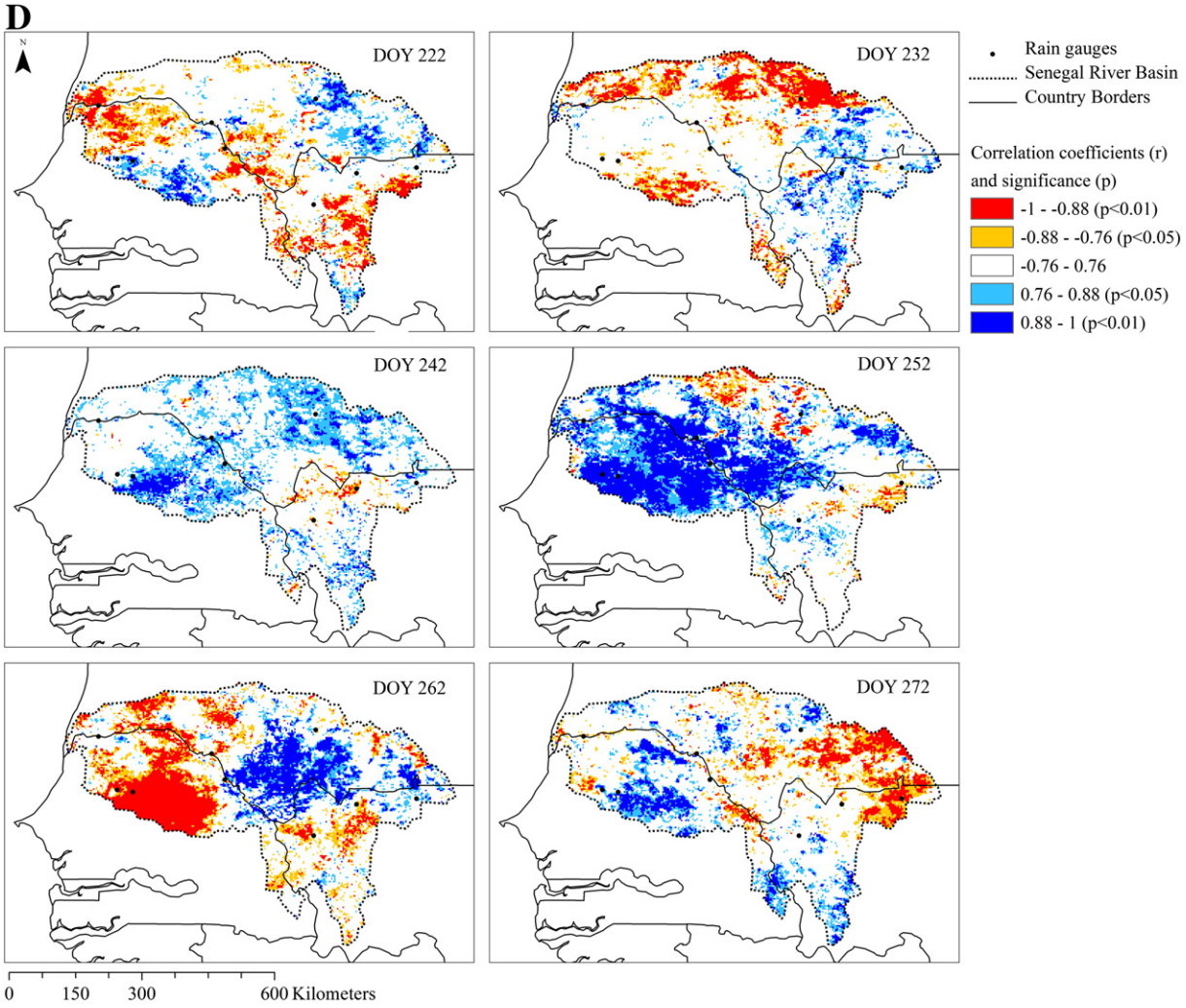

Fig. 7 (*continued*).

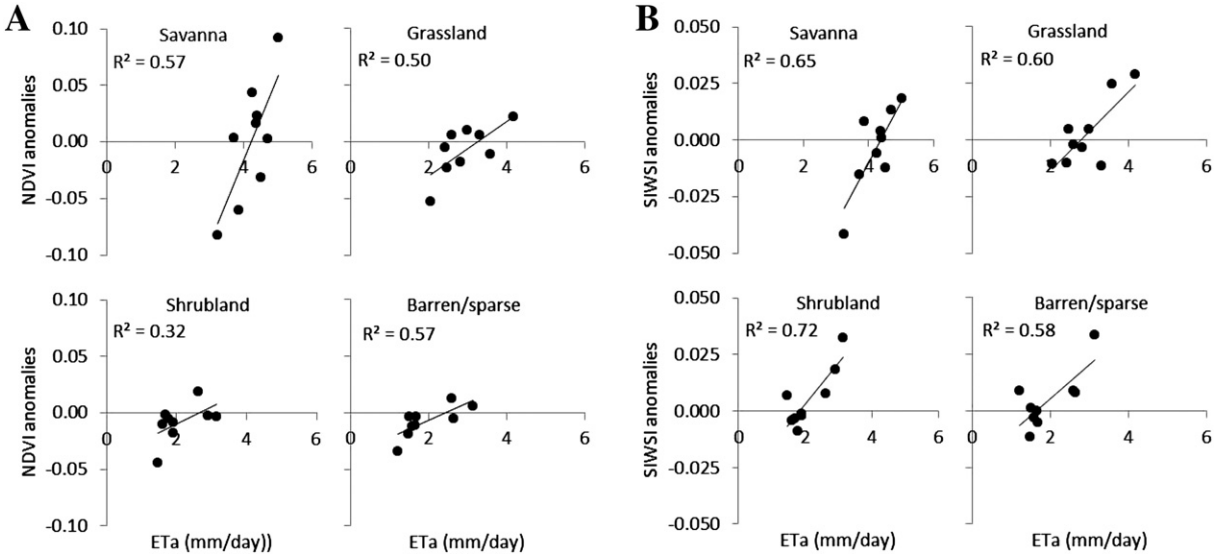

Fig. 8. A–B: X-axis: 10-day averages of modeled actual evapotranspiration (mm/day). Y-axis: 7 day fitted change of NDVI anomalies (A) or 7 day fitted change of SIWSI anomalies (B). Values are derived with 10-day time intervals, starting at DOY 192 and ending DOY 272 (2008), and averaged for each Land Cover Class (LCC).

the need of seasonal detrending. Finally, the possibilities for combining short term variations of anomalies from NIR/SWIR indices with Thermal Infrared (TIR) information should be examined, where geostationary remote sensing also provides great potential for observing vegetation stress.

References

Abbott, M.B., Bathurst, J.C., Cunge, J.A., Oconnell, P.E., & Rasmussen, J. (1986). An introduction to the European Hydrological system — Systeme Hydrologique Europeen, She.2. Structure of a physically-based, distributed modeling system. *Journal of Hydrology*, *87*, 61–77.

Andersen, J., Refsgaard, J.C., & Jensen, K.H. (2001). Distributed hydrological modelling of the Senegal River Basin — model construction and validation. *Journal of Hydrology*, *247*, 200–214.

Anyamba, A., & Tucker, C.J. (2005). Analysis of Sahelian vegetation dynamics using NOAA-AVHRR NDVI data from 1981-2003. *Journal of Arid Environments*, *63*, 596–614.

Breman, H., & Dewit, C.T. (1983). Rangeland productivity and exploitation in the Sahel. *Science*, *221*, 1341–1347.

Carlson, T.N., & Ripley, D.A. (1994). *A method to make use of thermal infrared temperature and NDVI measurements to infer surface soil water content and fractional vegetation cover, 161–173 (173 pp.).*

Carlson, T.N., & Ripley, D.A. (1997). On the relation between NDVI, fractional vegetation cover, and leaf area index. *Remote Sensing of Environment*, *62*, 241–252.

Ceccato, P., Flasse, S., & Gregoire, J.M. (2002). Designing a spectral index to estimate vegetation water content from remote sensing data — Part 2. Validation and applications. *Remote Sensing of Environment*, *82*, 198–207.

Ceccato, P., Flasse, S., Tarantola, S., Jacquemoud, S., & Gregoire, J.M. (2001). Detecting vegetation leaf water content using reflectance in the optical domain. *Remote Sensing of Environment*, *77*, 22–33.

Ceccato, P., Gobron, N., Flasse, S., Pinty, B., & Tarantola, S. (2002). Designing a spectral index to estimate vegetation water content from remote sensing data: Part 1 — Theoretical approach. *Remote Sensing of Environment*, *82*, 188–197.

D'Errico, J. (2004). Surface Fitting using inpaint_nans. http://www.mathworks.com/matlabcentral/fileexchange/4551-inpaint-nans (Updated 2012. MATLAB Central File Exchange, retrieved 2013)

Dinku, T., Chidzambwa, S., Ceccato, P., Connor, S.J., & Ropelewski, C.F. (2008). Validation of high-resolution satellite rainfall products over complex terrain. *International Journal of Remote Sensing*, *29*, 4097–4110.

Duan, Q.Y., Sorooshian, S., & Gupta, V. (1992). Effective and efficient global optimization for conceptual rainfall–runoff models. *Water Resources Research*, *28*, 1015–1031.

Elberse, W.T., & Breman, H. (1989). Germination and establishment of Sahelian rangeland species.1. Seed properties. *Oecologia*, *80*, 477–484.

Elberse, W.T., & Breman, H. (1990). Germination and establishment of Sahelian rangeland species II. Effects of water availability. *Oecologia*, *85*, 32–40.

Fensholt, R., Huber, S., Proud, S.R., & Mbow, C. (2010). Detecting canopy water status using shortwave infrared reflectance data from polar orbiting and geostationary platforms. *Ieee Journal of Selected Topics in Applied Earth Observations and Remote Sensing*, *3*, 271–285.

Fensholt, R., Langanke, T., Rasmussen, K., Reenberg, A., Prince, S.D., Tucker, C., et al. (2012). Greenness in semi-arid areas across the globe 1981-2007 — an Earth Observing Satellite based analysis of trends and drivers. *Remote Sensing of Environment*, *121*, 144–158.

Fensholt, R., & Proud, S.R. (2012). Evaluation of Earth Observation based global long term vegetation trends — comparing GIMMS and MODIS global NDVI time series. *Remote Sensing of Environment*, *119*, 131–147.

Fensholt, R., & Sandholt, I. (2003). Derivation of a shortwave infrared water stress index from MODIS near- and shortwave infrared data in a semiarid environment. *Remote Sensing of Environment*, *87*, 111–121.

Fensholt, R., Sandholt, I., Proud, S.R., Stisen, S., & Rasmussen, M.O. (2010). Assessment of MODIS sun-sensor geometry variations effect on observed NDVI using MSG SEVIRI geostationary data. *International Journal of Remote Sensing*, *31*, 6163–6187.

Fensholt, R., Sandholt, I., Rasmussen, M.S., Stisen, S., & Diouf, A. (2006). Evaluation of satellite based primary production modelling in the semi-arid Sahel. *Remote Sensing of Environment*, *105*, 173–188.

Gao, B.C. (1996). NDWI — a normalized difference water index for remote sensing of vegetation liquid water from space. *Remote Sensing of Environment*, *58*, 257–266.

Gillies, R.R., Carlson, T.N., Cui, J., Kustas, W.P., & Humes, K.S. (1997). A verification of the 'triangle' method for obtaining surface soil water content and energy fluxes from remote measurements of the Normalized Difference Vegetation Index (NDVI) and surface radiant temperature. *International Journal of Remote Sensing*, *18*, 3145–3166.

Herman, A., Kumar, V.B., Arkin, P.A., & Kousky, J.V. (1997). Objectively determined 10-day African rainfall estimates created for famine early warning systems. *International Journal of Remote Sensing*, *18*, 2147–2159.

Heumann, B.W., Seaquist, J.W., Eklundh, L., & Jonsson, P. (2007). AVHRR derived phenological change in the Sahel and Soudan, Africa, 1982–2005. *Remote Sensing of Environment*, *108*, 385–392.

Jonsson, P., & Eklundh, L. (2004). TIMESAT — a program for analyzing time-series of satellite sensor data. *Computers & Geosciences*, *30*, 833–845.

Ju, J.C., Roy, D.P., Shuai, Y.M., & Schaaf, C. (2010). Development of an approach for generation of temporally complete daily nadir MODIS reflectance time series. *Remote Sensing of Environment*, *114*, 1–20.

Julien, Y., & Sobrino, J.A. (2009). Global land surface phenology trends from GIMMS database. *International Journal of Remote Sensing*, *30*, 3495–3513.

Kogan, F.N. (1995). Application of vegetation index and brightness temperature for drought detection. *Natural Hazards: Monitoring and Assessment Using Remote Sensing Technique*, *15*, 91–100.

Kristensen, K.J., & Jensen, S.E. (1975). A model for estimation the actual evapotranspiration from the potential one. *Nordic Hydrology*, *6*, 170–188.

Lutz, H.J. (2009). *Cloud Detection for MSG — algorithm theoretical basis document (ATBD). EUMETSAT: EUMETSAT.*

Mbow, C., Fensholt, R., Rasmussen, K., & Diop, D. (2013). Can vegetation productivity be derived from greenness in a semi-arid environment? Evidence from ground based measurements. *Journal of Arid Environments*, *97*, 55–65.

Mertz, O., D'haen, S., Maiga, A., Moussa, I.B., Barbier, B., Diouf, A., et al. (2012). Climate variability and environmental stress in the Sudan-Sahel zone of West Africa. *Ambio*, *41*, 380–392.

Morton, D.C., Nagol, J., Carabajal, C.C., Rosette, J., Palace, M., Cook, B.D., et al. (2014). Amazon forests maintain consistent canopy structure and greenness during the dry season. *Nature*, *506* (221-+).

Nicholson, S.E., Davenport, M.L., & Malo, A.R. (1990). A comparison of the vegetation response to rainfall in the Sahel and East-Africa, using normalized difference vegetation index from Noaa Avhrr. *Climatic Change*, *17*, 209–241.

Olsen, J.L., Ceccato, P., Proud, S.R., Fensholt, R., Grippa, M., Mougin, E., et al. (2013). Relation between seasonally detrended shortwave infrared reflectance data and land surface moisture in semi-arid Sahel. *Remote Sensing*, *5*, 2898–2927.

Pierre, C., Bergametti, G., Marticorena, B., Mougin, E., Lebel, T., & Ali, A. (2011). Pluriannual comparisons of satellite-based rainfall products over the Sahelian belt for seasonal vegetation modeling. *Journal of Geophysical Research-Atmospheres*, *116*.

Prince, S.D. (1991a). A model of regional primary production for use with coarse resolution satellite data. *International Journal of Remote Sensing*, *12*, 1313–1330.

Prince, S.D. (1991b). Satellite remote-sensing of primary production — comparison of results for Sahelian Grasslands 1981–1988. *International Journal of Remote Sensing*, *12*, 1301–1311.

Proud, S.R., & Rasmussen, L.V. (2010). The influence of seasonal rainfall upon Sahel vegetation. *Remote Sensing Letters*, *2*, 241–249.

Proud, S.R., Rasmussen, M.O., Fensholt, R., Sandholt, I., Shisanya, C., Mutero, W., et al. (2010). Improving the SMAC atmospheric correction code by analysis of Meteosat Second Generation NDVI and surface reflectance data. *Remote Sensing of Environment*, *114*, 1687–1698.

Proud, S.R., Zhanf, Q., Schaaf, C., Fensholt, R., Rasmussen, M.O., Shisanya, C., et al. (2014). *The Normalization of the Surface Anisotropy Effects Present in SEVIRI Reflectance Data by Using the MODIS BRDF Method.*

Rahman, H., & Dedieu, G. (1994). Smac — a simplified method for the atmospheric correction of satellite measurements in the solar spectrum. *International Journal of Remote Sensing*, *15*, 123–143.

Rojas, O., Vrieling, A., & Rembold, F. (2011). Assessing drought probability for agricultural areas in Africa with coarse resolution remote sensing imagery. *Remote Sensing of Environment*, *115*, 343–352.

Sandholt, I., Rasmussen, K., & Andersen, J. (2002). A simple interpretation of the surface temperature/vegetation index space for assessment of surface moisture status. *Remote Sensing of Environment*, *79*, 213–224.

Schaaf, C. B., Gao, F., Strahler, A. H., Lucht, W., Li, X.W., Tsang, T., et al. (2002). First operational BRDF, albedo nadir reflectance products from MODIS. *Remote Sensing of Environment*, *83*, 135–148.

Schmetz, J., Pili, P., Tjemkes, S., Just, D., Kerkmann, J., Rota, S., et al. (2002). An introduction to Meteosat Second Generation (MSG). *Bulletin of the American Meteorological Society*, *83* (977-+).

Sobrino, J.A., & Julien, Y. (2011). Global trends in NDVI-derived parameters obtained from GIMMS data. *International Journal of Remote Sensing*, *32*, 4267–4279.

Stisen, S., Jensen, K.H., Sandholt, I., & Grimes, D.I.F. (2008). A remote sensing driven distributed hydrological model of the Senegal River basin. *Journal of Hydrology*, *354*, 131–148.

Stisen, S., & Sandholt, I. (2010). Evaluation of remote-sensing-based rainfall products through predictive capability in hydrological runoff modelling. *Hydrological Processes*, *24*, 879–891.

Thiemig, V., Rojas, R., Zambrano-Bigiarini, M., Levizzani, V., & De Roo, A. (2012). Validation of satellite-based precipitation products over sparsely gauged African River Basins. *Journal of Hydrometeorology*, *13*, 1760–1783.

Tucker, C.J. (1978). Comparison of satellite sensor bands for vegetation monitoring. *Photogrammetric Engineering and Remote Sensing*, *44*, 1369–1380.

Tucker, C.J. (1979). Red and photographic infrared linear combinations for monitoring vegetation. *Remote Sensing of Environment*, *8*, 127–150.

Tucker, C.J. (1980). Remote-sensing of leaf water-content in the near-infrared. *Remote Sensing of Environment*, *10*, 23–32.

Wang, J., Rich, P.M., & Price, K.P. (2003). Temporal responses of NDVI to precipitation and temperature in the central Great Plains, USA. *International Journal of Remote Sensing*, *24*, 2345–2364.

Zhao, M., Running, S.W., & Nemani, R.R. (2006). Sensitivity of Moderate Resolution Imaging Spectroradiometer (MODIS) terrestrial primary production to the accuracy of meteorological reanalyses. *Journal of Geophysical Research-Biogeosciences*, *111*.